Ultrahigh Energy Neutrinos
at the Pierre Auger Observatory

The Pierre Auger Collaboration [*]

April 8, 2013

[*]Correspondence to The Pierre Auger Collaboration; auger spokesperson@fnal.gov

1

The Pierre Auger Collaboration

P. Abreu[65], M. Aglietta[53], M. Ahlers[95], E.J. Ahn[83], I.F.M. Albuquerque[16], D. Allard[30], I. Allekotte[1], J. Allen[87], P. Allison[89], A. Almela[11, 7], J. Alvarez Castillo[58], J. Alvarez-Muñiz[75], R. Alves Batista[17], M. Ambrosio[47], A. Aminaei[59], L. Anchordoqui[96], S. Andringa[65], T. Antiči'c[24], C. Aramo[47], E. Arganda[4, 72], F. Arqueros[72], H. Asorey[1], P. Assis[65], J. Aublin[32], M. Ave[38], M. Avenier[33], G. Avila[10], T. Bäcker[42], A.M. Badescu[68], M. Balzer[37], K.B. Barber[12], A.F. Barbosa[14] ‡, R. Bardenet[31], S.L.C. Barroso[19], B. Baughman[89] f, J. Bäuml[36], J.J. Beatty[89], B.R. Becker[94], K.H. Becker[35], A. Bellétoile[34], J.A. Bellido[12], S. BenZvi[95], C. Berat[33], X. Bertou[1], P.L. Biermann[39], P. Billoir[32], F. Blanco[72], M. Blanco[32, 73], C. Bleve[35], H. Blümer[38, 36], M. Boháčová[26], D. Boncioli[48], C. Bonifazi[22, 32], R. Bonino[53], N. Borodai[63], J. Brack[81], I. Brancus[66], P. Brogueira[65], W.C. Brown[82], R. Bruijn[77] i, P. Buchholz[42], A. Bueno[74], R.E. Burton[79], K.S. Caballero-Mora[90], B. Caccianiga[45], L. Caramete[39], R. Caruso[49], A. Castellina[53], O. Catalano[52], G. Cataldi[46], L. Cazon[65], R. Cester[50], J. Chauvin[33], S.H. Cheng[90], A. Chiavassa[53], J.A. Chinellato[17], J. Chirinos Diaz[86], J. Chudoba[26], M. Cilmo[47], R.W. Clay[12], M.R. Coluccia[46], R. Conceição[65], F. Contreras[9], H. Cook[77], M.J. Cooper[12], J. Coppens[59, 61], A. Cordier[31], S. Coutu[90], C.E. Covault[79], A. Creusot[30], A. Criss[90], J. Cronin[92], A. Curutiu[39], S. Dagoret-Campagne[31], R. Dallier[34], B. Daniel[17], S. Dasso[5, 3], K. Daumiller[36], B.R. Dawson[12], R.M. de Almeida[23], M. De Domenico[49], C. De Donato[58], S.J. de Jong[59, 61], G. De La Vega[8], W.J.M. de Mello Junior[17], J.R.T. de Mello Neto[22], I. De Mitri[46], V. de Souza[15], K.D. de Vries[60], L. del Peral[73], M. del Río[48, 9], O. Deligny[29], H. Dembinski[38], N. Dhital[86], C. Di Giulio[48, 44], M.L. Díaz Castro[14], P.N. Diep[97], F. Diogo[65], C. Dobrigkeit [17], W. Docters[60], J.C. D'Olivo[58], P.N. Dong[97, 29], A. Dorofeev[81], J.C. dos Anjos[14], M.T. Dova[4], D. D'Urso[47], I. Dutan[39], J. Ebr[26], R. Engel[36], M. Erdmann[40], C.O. Escobar[83, 17], J. Espadanal[65], A. Etchegoyen[7, 11], P. Facal San Luis[92], H. Falcke[59, 62], G. Farrar[87], A.C. Fauth[17], N. Fazzini[83], A.P. Ferguson[79], B. Fick[86], A. Filevich[7], A. Filipčič[69, 70], S. Fliescher[40], C.E. Fracchiolla[81], E.D. Fraenkel[60], O. Fratu[68], U. Fröhlich[42], B. Fuchs[38], R. Gaior[32], R.F. Gamarra[7], S. Gambetta[43], B. García[8], S.T. Garcia Roca[75], D. Garcia-Gamez[31], D. Garcia-Pinto[72], A. Gascon Bravo[74], H. Gemmeke[37], P.L. Ghia[32], M. Giller[64], J. Gitto[8], H. Glass[83], M.S. Gold[94], G. Golup[1], F. Gomez Albarracin[4], M. Gómez Berisso[1], P.F. Gómez Vitale[10], P. Gonçalves[65], J.G. Gonzalez[36], B. Gookin[81], A. Gorgi[53], P. Gouffon[16], E. Grashorn[89], S. Grebe[59, 61], N. Griffith[89], M. Grigat[40], A.F. Grillo[54], Y. Guardincerri[3], F. Guarino[47], G.P. Guedes[18], P. Hansen[4], D. Harari[1], T.A. Harrison[12], J.L. Harton[81], A. Haungs[36], T. Hebbeker[40], D. Heck[36], A.E. Herve[12], C. Hojvat[83], N. Hollon[92], V.C. Holmes[12], P. Homola[63], J.R. Hörandel[59], P. Horvath[27], M. Hrabovský[27, 26], D. Huber[38], T. Huege[36], A. Insolia[49], F. Ionita[92], A. Italiano[49], C. Jarne[4], S. Jiraskova[59], M. Josebachuili[7], K. Kadija[24], K.H. Kampert[35], P. Karhan[25], P. Kasper[83], I. Katkov[38], B. Kégl[31], B. Keilhauer[36], A. Keivani[85], J.L. Kelley[59], E. Kemp[17], R.M. Kieckhafer[86], H.O. Klages[36], M. Kleifges[37], J. Kleinfeller[9, 36], J. Knapp[77], D.-H. Koang[33], K. Kotera[92], N. Krohm[35],

O. Krömer[37], D. Kruppke-Hansen[35], F. Kuehn[83], D. Kuempel[40, 42], J.K. Kulbartz[41], N. Kunka[37], G. La Rosa[52], C. Lachaud[30], D. LaHurd[79], L. Latronico[53], R. Lauer[94], P. Lautridou[34], S. Le Coz[33], M.S.A.B. Leão[21], D. Lebrun[33], P. Lebrun[83], M.A. Leigui de Oliveira[21], A. Letessier-Selvon[32], I. Lhenry-Yvon[29], K. Link[38], R. López[55], A. Lopez Agüera[75], K. Louedec[33, 31], J. Lozano Bahilo[74], L. Lu[77], A. Lucero[7], M. Ludwig[38], H. Lyberis[22, 29], M.C. Maccarone[52], C. Macolino[32], S. Maldera[53], D. Mandat[26], P. Mantsch[83], A.G. Mariazzi[4], J. Marin[9, 53], V. Marin[34], I.C. Maris[32], H.R. Marquez Falcon[57], G. Marsella[51], D. Martello[46], L. Martin[34], H. Martinez[56], O. Martínez Bravo[55], H.J. Mathes[36], J. Matthews[85, 91], J.A.J. Matthews[94], G. Matthiae[48], D. Maurel[36], D. Maurizio[50], P.O. Mazur[83], G. Medina-Tanco[58], M. Melissas[38], D. Melo[7], E. Menichetti[50], A. Menshikov[37], P. Mertsch[76], C. Meurer[40], S. Mi'canovi'c[24], M.I. Micheletti[6], I.A. Minaya[72], L. Miramonti[45], L. Molina-Bueno[74], S. Mollerach[1], M. Monasor[92], D. Monnier Ragaigne[31], F. Montanet[33], B. Morales[58], C. Morello[53], E. Moreno[55], J.C. Moreno[4], M. Mostafá[81], C.A. Moura[21], M.A. Muller[17], G. Müller[40], M. Münchmeyer[32], R. Mussa[50], G. Navarra[53] ‡, J.L. Navarro[74], S. Navas[74], P. Necesal[26], L. Nellen[58], A. Nelles[59, 61], J. Neuser[35], P.T. Nhung[97], M. Niechciol[42], L. Niemietz[35], N. Nierstenhoefer[35], D. Nitz[86], D. Nosek[25], L. Nožka[26], J. Oehlschläger[36], A. Olinto[92], M. Ortiz[72], N. Pacheco[73], D. Pakk Selmi-Dei[17], M. Palatka[26], J. Pallotta[2], N. Palmieri[38], G. Parente[75], E. Parizot[30], A. Parra[75], S. Pastor[71], T. Paul[88], M. Pech[26], J. Pękala[63], R. Pelayo[55, 75], I.M. Pepe[20], L. Perrone[51], R. Pesce[43], E. Petermann[93], S. Petrera[44], A. Petrolini[43], Y. Petrov[81], C. Pfendner[95], R. Piegaia[3], T. Pierog[36], P. Pieroni[3], M. Pimenta[65], V. Pirronello[49], M. Platino[7], M. Plum[40], V.H. Ponce[1], M. Pontz[42], A. Porcelli[36], P. Privitera[92], M. Prouza[26], E.J. Quel[2], S. Querchfeld[35], J. Rautenberg[35], O. Ravel[34], D. Ravignani[7], B. Revenu[34], J. Ridky[26], S. Riggi[75], M. Risse[42], P. Ristori[2], H. Rivera[45], V. Rizi[44], J. Roberts[87], W. Rodrigues de Carvalho[75], G. Rodriguez[75], I. Rodriguez Cabo[75], J. Rodriguez Martino[9], J. Rodriguez Rojo[9], M.D. Rodríguez-Frías[73], G. Ros[73], J. Rosado[72], T. Rossler[27], M. Roth[36], B. Rouillé-d'Orfeuil[92], E. Roulet[1], A.C. Rovero[5], C. Rühle[37], A. Saftoiu[66], F. Salamida[29], H. Salazar[55], F. Salesa Greus[81], G. Salina[48], F. Sánchez[7], C.E. Santo[65], E. Santos[65], E.M. Santos[22], F. Sarazin[80], B. Sarkar[35], S. Sarkar[76], R. Sato[9], N. Scharf[40], V. Scherini[45], H. Schieler[36], P. Schiffer[41, 40], A. Schmidt[37], O. Scholten[60], H. Schoorlemmer[59, 61], J. Schovancova[26], P. Schovánek[26], F. Schröder[36], S. Schulte[40], D. Schuster[80], S.J. Sciutto[4], M. Scuderi[49], A. Segreto[52], M. Settimo[42], A. Shadkam[85], R.C. Shellard[14], I. Sidelnik[7], G. Sigl[41], H.H. Silva Lopez[58], O. Sima[67], A. 'Smiałkowski[64], R. Šmída[36], G.R. Snow[93], P. Sommers[90], J. Sorokin[12], H. Spinka[78, 83], R. Squartini[9], Y.N. Srivastava[88], S. Stanic[70], J. Stapleton[89], J. Stasielak[63], M. Stephan[40], A. Stutz[33], F. Suarez[7], T. Suomijärvi[29], A.D. Supanitsky[5], T. Šuša[24], M.S. Sutherland[85], J. Swain[88], Z. Szadkowski[64], M. Szuba[36], A. Tapia[7], M. Tartare[33], O. Taşcău[35], R. Tcaciuc[42], N.T. Thao[97], D. Thomas[81], J. Tiffenberg[3], C. Timmermans[61, 59], W. Tkaczyk[64] ‡, C.J. Todero Peixoto[15], G. Toma[66], L. Tomankova[26], B. Tomé[65], A. Tonachini[50], P. Travnicek[26], D.B. Tridapalli[16], G. Tristram[30], E. Trovato[49], M. Tueros[75], R. Ulrich[36],

3

M. Unger[36], M. Urban[31], J.F. Valdés Galicia[58], I. Valiño[75], L. Valore[47], A.M. van den Berg[60], E. Varela[55], B. Vargas Cárdenas[58], J.R. Vázquez[72], R.A. Vázquez[75], D. Veberič[70, 69], V. Verzi[48], J. Vicha[26], M. Videla[8], L. Villaseñor[57], H. Wahlberg[4], P. Wahrlich[12], O. Wainberg[7, 11], D. Walz[40], A.A. Watson[77], M. Weber[37], K. Weidenhaupt[40], A. Weindl[36], F. Werner[36], S. Westerhoff[95], B.J. Whelan[12], A. Widom[88], G. Wieczorek[64], L. Wiencke[80], B. Wilczyńska[63], H. Wilczyński[63], M. Will[36], C. Williams[92], T. Winchen[40], M. Wommer[36], B. Wundheiler[7], T. Yamamoto[92] [a], T. Yapici[86], P. Younk[42, 84], G. Yuan[85], A. Yushkov[75], B. Zamorano Garcia[74], E. Zas[75], D. Zavrtanik[70, 69], M. Zavrtanik[69, 70], I. Zaw[87] [h], A. Zepeda[56], Y. Zhu[37], M. Zimbres Silva[35, 17], M. Ziolkowski[42]

[1] Centro Atómico Bariloche and Instituto Balseiro (CNEA-UNCuyo-CONICET), San Carlos de Bariloche, Argentina
[2] Centro de Investigaciones en Láseres y Aplicaciones, CITEDEF and CONICET, Argentina
[3] Departamento de Física, FCEyN, Universidad de Buenos Aires y CONICET, Argentina
[4] IFLP, Universidad Nacional de La Plata and CONICET, La Plata, Argentina
[5] Instituto de Astronomía y Física del Espacio (CONICET-UBA), Buenos Aires, Argentina
[6] Instituto de Física de Rosario (IFIR) - CONICET/U.N.R. and Facultad de Ciencias Bioquímicas y Farmacéuticas U.N.R., Rosario, Argentina
[7] Instituto de Tecnologías en Detección y Astropartículas (CNEA, CONICET, UNSAM), Buenos Aires, Argentina
[8] National Technological University, Faculty Mendoza (CONICET/CNEA), Mendoza, Argentina
[9] Observatorio Pierre Auger, Malargüe, Argentina
[10] Observatorio Pierre Auger and Comisión Nacional de Energía Atómica, Malargüe, Argentina
[11] Universidad Tecnológica Nacional - Facultad Regional Buenos Aires, Buenos Aires, Argentina
[12] University of Adelaide, Adelaide, S.A., Australia
[14] Centro Brasileiro de Pesquisas Fisicas, Rio de Janeiro, RJ, Brazil
[15] Universidade de São Paulo, Instituto de Física, São Carlos, SP, Brazil
[16] Universidade de São Paulo, Instituto de Física, São Paulo, SP, Brazil
[17] Universidade Estadual de Campinas, IFGW, Campinas, SP, Brazil
[18] Universidade Estadual de Feira de Santana, Brazil
[19] Universidade Estadual do Sudoeste da Bahia, Vitoria da Conquista, BA, Brazil
[20] Universidade Federal da Bahia, Salvador, BA, Brazil
[21] Universidade Federal do ABC, Santo André, SP, Brazil
[22] Universidade Federal do Rio de Janeiro, Instituto de Física, Rio de Janeiro, RJ, Brazil

[23] Universidade Federal Fluminense, EEIMVR, Volta Redonda, RJ, Brazil
[24] Rudjer Boškovi'c Institute, 10000 Zagreb, Croatia
[25] Charles University, Faculty of Mathematics and Physics, Institute of Particle and Nuclear Physics, Prague, Czech Republic
[26] Institute of Physics of the Academy of Sciences of the Czech Republic, Prague, Czech Republic
[27] Palacky University, RCPTM, Olomouc, Czech Republic
[29] Institut de Physique Nucléaire d'Orsay (IPNO), Université Paris 11, CNRS-IN2P3, Orsay, France
[30] Laboratoire AstroParticule et Cosmologie (APC), Université Paris 7, CNRS-IN2P3, Paris, France
[31] Laboratoire de l'Accélérateur Linéaire (LAL), Université Paris 11, CNRS-IN2P3, Orsay, France
[32] Laboratoire de Physique Nucléaire et de Hautes Energies (LPNHE), Universités Paris 6 et Paris 7, CNRS-IN2P3, Paris, France
[33] Laboratoire de Physique Subatomique et de Cosmologie (LPSC), Université Joseph Fourier, INPG, CNRS-IN2P3, Grenoble, France
[34] SUBATECH, École des Mines de Nantes, CNRS-IN2P3, Université de Nantes, Nantes, France
[35] Bergische Universität Wuppertal, Wuppertal, Germany
[36] Karlsruhe Institute of Technology - Campus North - Institut für Kernphysik, Karlsruhe, Germany
[37] Karlsruhe Institute of Technology - Campus North - Institut für Prozessdatenverarbeitung und Elektronik, Karlsruhe, Germany
[38] Karlsruhe Institute of Technology - Campus South - Institut für Experimentelle Kernphysik (IEKP), Karlsruhe, Germany
[39] Max-Planck-Institut für Radioastronomie, Bonn, Germany
[40] RWTH Aachen University, III. Physikalisches Institut A, Aachen, Germany
[41] Universität Hamburg, Hamburg, Germany
[42] Universität Siegen, Siegen, Germany
[43] Dipartimento di Fisica dell'Università and INFN, Genova, Italy
[44] Università dell'Aquila and INFN, L'Aquila, Italy
[45] Università di Milano and Sezione INFN, Milan, Italy
[46] Dipartimento di Fisica dell'Università del Salento and Sezione INFN, Lecce, Italy
[47] Università di Napoli "Federico II" and Sezione INFN, Napoli, Italy
[48] Università di Roma II "Tor Vergata" and Sezione INFN, Roma, Italy
[49] Università di Catania and Sezione INFN, Catania, Italy
[50] Università di Torino and Sezione INFN, Torino, Italy
[51] Dipartimento di Ingegneria dell'Innovazione dell'Università del Salento and Sezione INFN, Lecce, Italy
[52] Istituto di Astrofisica Spaziale e Fisica Cosmica di Palermo (INAF), Palermo, Italy

[53] Istituto di Fisica dello Spazio Interplanetario (INAF), Università di Torino and Sezione INFN, Torino, Italy
[54] INFN, Laboratori Nazionali del Gran Sasso, Assergi (L'Aquila), Italy
[55] Benemérita Universidad Autónoma de Puebla, Puebla, Mexico
[56] Centro de Investigación y de Estudios Avanzados del IPN (CINVESTAV), México, D.F., Mexico
[57] Universidad Michoacana de San Nicolas de Hidalgo, Morelia, Michoacan, Mexico
[58] Universidad Nacional Autonoma de Mexico, Mexico, D.F., Mexico
[59] IMAPP, Radboud University Nijmegen, Netherlands
[60] Kernfysisch Versneller Instituut, University of Groningen, Groningen, Netherlands
[61] Nikhef, Science Park, Amsterdam, Netherlands
[62] ASTRON, Dwingeloo, Netherlands
[63] Institute of Nuclear Physics PAN, Krakow, Poland
[64] University of Łódź, Łódź, Poland
[65] LIP and Instituto Superior Técnico, Technical University of Lisbon, Portugal
[66] 'Horia Hulubei' National Institute for Physics and Nuclear Engineering, Bucharest-Magurele, Romania
[67] University of Bucharest, Physics Department, Romania
[68] University Politehnica of Bucharest, Romania
[69] J. Stefan Institute, Ljubljana, Slovenia
[70] Laboratory for Astroparticle Physics, University of Nova Gorica, Slovenia
[71] Instituto de Física Corpuscular, CSIC-Universitat de València, Valencia, Spain
[72] Universidad Complutense de Madrid, Madrid, Spain
[73] Universidad de Alcalá, Alcalá de Henares (Madrid), Spain
[74] Universidad de Granada & C.A.F.P.E., Granada, Spain
[75] Universidad de Santiago de Compostela, Spain
[76] Rudolf Peierls Centre for Theoretical Physics, University of Oxford, Oxford, United Kingdom
[77] School of Physics and Astronomy, University of Leeds, United Kingdom
[78] Argonne National Laboratory, Argonne, IL, USA
[79] Case Western Reserve University, Cleveland, OH, USA
[80] Colorado School of Mines, Golden, CO, USA
[81] Colorado State University, Fort Collins, CO, USA
[82] Colorado State University, Pueblo, CO, USA
[83] Fermilab, Batavia, IL, USA
[84] Los Alamos National Laboratory, Los Alamos, NM, USA
[85] Louisiana State University, Baton Rouge, LA, USA
[86] Michigan Technological University, Houghton, MI, USA
[87] New York University, New York, NY, USA
[88] Northeastern University, Boston, MA, USA

[89] Ohio State University, Columbus, OH, USA
[90] Pennsylvania State University, University Park, PA, USA
[91] Southern University, Baton Rouge, LA, USA
[92] University of Chicago, Enrico Fermi Institute, Chicago, IL, USA
[93] University of Nebraska, Lincoln, NE, USA
[94] University of New Mexico, Albuquerque, NM, USA
[95] University of Wisconsin, Madison, WI, USA
[96] University of Wisconsin, Milwaukee, WI, USA
[97] Institute for Nuclear Science and Technology (INST), Hanoi, Vietnam

(‡) Deceased
(a) at Konan University, Kobe, Japan
(f) now at University of Maryland
(h) now at NYU Abu Dhabi
(i) now at Université de Lausanne

Abstract

The observation of ultrahigh energy neutrinos (UHEνs) has become a priority in experimental astroparticle physics. UHEνs can be detected with a variety of techniques. In particular, neutrinos can interact in the atmosphere (downward-going ν) or in the Earth crust (Earth-skimming ν), producing air showers that can be observed with arrays of detectors at the ground. With the Surface Detector Array of the Pierre Auger Observatory we can detect these types of cascades. The distinguishing signature for neutrino events is the presence of very inclined showers produced close to the ground (i.e. after having traversed a large amount of atmosphere). In this work we review the procedure and criteria established to search for UHEνs in the data collected with the ground array of the Pierre Auger Observatory. This includes Earth-skimming as well as downward-going neutrinos. No neutrino candidates have been found, which allows us to place competitive limits to the diffuse flux of UHEνs in the EeV range and above.

1. Introduction

The observation of ultrahigh energy cosmic rays (UHECR) of energy $1 - 100$ EeV ($10^{18} - 10^{20}$ eV) has stimulated much experimental as well as theoretical activity in the field of Astroparticle Physics [1, 2]. Although many mysteries remain to be solved, such as the origin of the UHECRs, their production mechanism and composition, we know that it is very difficult to produce these energetic particles without associated fluxes of ultrahigh energy neutrinos (UHEνs) [3].

In the so-called "bottom-up" models, protons and nuclei are accelerated in astrophysical shocks, where pions are believed to be produced by cosmic ray interactions with matter or radiation at the source [4]. In the so-called "top-down" scenarios, protons and neutrons are produced from quark and gluon fragmentation, a mechanism which is known to produce much more pions than nucleons [5]. Furthermore, protons and nuclei also produce pions in their unavoidable interactions responsible for the Greisen-Zatsepin-Kuzmin (GZK) cut-off [6, 7]. The flux of UHECRs above $\sim 5 \times 10^{19}$ eV is known to be largely suppressed with respect to that at lower energies, a feature seen in the UHECR spectrum [8, 9] that is compatible with the interaction of UHECRs with the cosmic microwave background (CMB) radiation. If the primaries are protons, the interaction responsible for the GZK effect is photopion production, and the decays of the charged pions produce UHE neutrinos. However, their fluxes are uncertain [4], and if the primaries are heavier nuclei, the UHEν yield would be strongly suppressed [10].

The observation of UHE neutrinos could provide important hints to the origin of UHECRs [11, 12]. Unlike cosmic rays, neutrinos point directly to the source where they were produced, without being deflected by Galactic

and extragalactic magnetic fields. Unlike photons they travel undisturbed from the sources carrying a footprint of the production model.

High energy neutrinos can be detected with a variety of techniques [13, 14]. In particular they can be observed with arrays of detectors at ground level that are currently being used to measure extensive showers produced by cosmic rays [15]. The main challenge in this technique lies in separating showers initiated by neutrinos from those induced by regular cosmic rays. It was suggested in the 1970s that this could be done at high zenith angles [16] because the atmosphere slant depth provides a quite large target for neutrino interactions. The idea is that neutrinos, having very small cross-sections, can interact at any point along their trajectories, while protons, nuclei or photons interact shortly after entering the atmosphere. The signature for neutrino events is thus inclined showers that interact deep in the atmosphere.

Inclined showers were first observed in the 1960s by several groups [17, 18]. With the Surface Detector Array (SD) of the Pierre Auger Observatory [19] we can detect inclined showers and identify neutrinos with energies typically above 0.1 EeV. There are two ways of performing this task:

1. Neutrinos of all flavours can collide with nuclei in the atmosphere and induce an extensive air shower close to the ground [20]. In this so-called "downward-going" neutrino channel, both charged current (CC) and neutral-current (NC) interactions contribute to the neutrino event rate.

2. Neutrinos of tau flavour (ν_τ) are expected to be most sensitively observed through the detection of showers induced by the decay products of an emerging τ lepton, after the propagation and interaction of an upward-going ν_τ inside the Earth [21, 22]. This "Earth-skimming" channel benefits from the long range of the τ lepton (~ 10 km for the shower energies relevant in this analysis) which sets the scale of the effective volume. Only charged-current interactions of ν_τ are relevant in this case.

In both the Earth-skimming and downward-going channels the showers can be identified and separated from cosmic ray induced showers with the SD of the Pierre Auger Observatory if the zenith angle is large enough, typically larger than $\sim 65°$–$75°$. A number of properties of the shower front, mostly stemming from the time distribution of the shower particles, can be used to distinguish neutrino-induced showers. As shown in Sec. 5, even though the criteria to identify neutrinos in both channels being based on similar ideas and variables, two different analyses were designed. The main reason for that concerns background reduction. The Earth-skimming neutrino search is restricted to a very narrow angular range where the background of nucleonic showers is expected to be very small. On the other hand in the broader

angular range of the downward-going neutrino search the background contamination is expected to be larger, and the selection criteria need to be more restrictive. This calls for specific algorithms and methods, capable of optimizing the separation of neutrino-induced showers from nucleonic ones as will be explained later in the paper.

In this work we review the procedure to search for UHEνs with the SD of the Auger Observatory, for both the Earth-skimming and downward-going channels. In Sec. 2 we give a brief overview of the SD of the Pierre Auger Observatory. In Sec. 3 we concentrate on the general strategy to search for UHEνs. Sec. 4 is devoted to describe the simulations of neutrino-induced showers crucial to establish selection criteria and to compute the exposure to UHEνs which is reported in Sec. 6. In Sec. 5 we give a detailed description of the neutrino selection criteria. When these criteria are applied blindly to the data collected at the SD no candidates are found. The resulting limits to the diffuse flux of UHEνs are presented in Sec. 7. Finally, in Sec. 8 we summarize the paper and give some prospects for future observations.

2.   The Pierre Auger Observatory

The Pierre Auger Observatory [19] is a hybrid UHECR detector combining an array of particle detectors at ground level, and 24 fluorescence telescopes housed in four buildings, for redundancy and calibration. It is located near the town of Malargüe, in the province of Mendoza in Argentina. In this review we focus on the surface detector array [19, 23] which is briefly described in the following.

2.1.   The Surface Detector Array

The surface detector array [23] consists of water Cherenkov detectors in the form of cylinders of 3.6 m diameter and 1.2 m height, each containing 12 tonnes of purified water. Charged particles entering the station emit Cherenkov light which is reflected at the walls by a diffusive Tyvek liner, and collected by three 9-inch photomultiplier tubes (PMT) at the top surface and in optical contact with the water. The PMT signals are sampled by flash analog to digital converters (FADC) with a time resolution of 25 ns. Each station is regularly monitored and calibrated in units of vertical equivalent muons (VEM) corresponding to the signal produced by a muon traversing the tank vertically through its center [24]. In Fig. 1 we show a picture of one of the water Cherenkov stations. The stations are autonomous, with all their components (PMTs, local processor, GPS receiver and radio system) powered by batteries coupled to solar panels. Once installed, the local stations work continuously without external intervention.

The SD was completed in 2008. There are ~ 1600 water stations arranged in a triangular grid with 1.5 km spacing between them, spanning
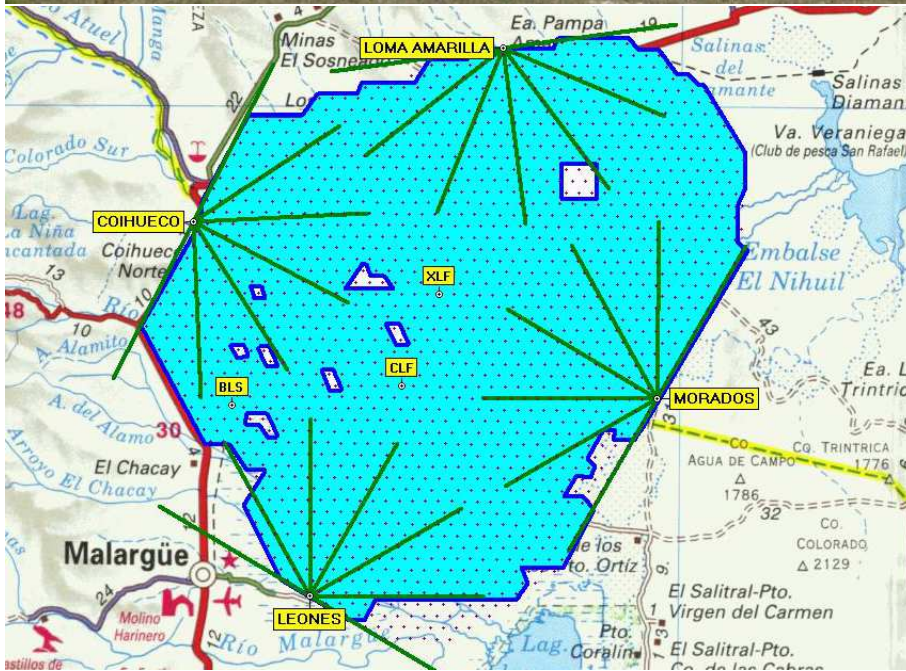
Figure 1: Top panel: one of the $\sim$ 1600 water Cherenkov stations that constitute the surface detector array of the Pierre Auger Observatory (forefront), and one of the four fluorescence buildings housing six of the 24 fluorescence telescopes (background). Bottom panel: Layout of the SD array with $\sim$ 1600 water Cherenkov stations (depicted as dots), spread over a surface of $\sim$ 3000 km^2 (blue area), with a distance between stations of 1.5 km. The four fluorescence buildings at the edges of the Observatory are also indicated.

an almost flat surface of ~ 3000 km^2, at an approximate altitude of 1400 m above sea level, or equivalently an atmospheric depth $X_{\mathrm{ground}} = 880$ g cm^{-2}. The layout of the SD array is sketched in the bottom panel of Fig. 1.

2.2. Surface Detector trigger

The stations transmit information by conventional radio links to the Central Data Acquisition System (CDAS) located in Malargüe. There are two types of trigger conditions. A local trigger at the level of an individual station (second order or T2 trigger), and a global trigger (third order or T3 trigger). The T2 trigger condition is the logical OR of two conditions: either a given threshold signal (3.2 VEM) is passed in at least one time bin of the FADC trace –the so-called "Threshold trigger"–, or a somewhat lower threshold (0.2 VEM) is passed in at least 13 bins within a 3 μs time window (i.e. 120 bins) –the so-called "Time-over-Threshold (ToT) trigger". The ToT condition was designed to trigger on signals broad in time, characteristic of the early stages of the development of an extensive air shower, and is crucial for neutrino identification as explained below. The data acquisition system receives the local T2 triggers and builds a global T3 trigger requiring a relatively compact configuration of at least three local stations compatible in time, each satisfying the ToT trigger, or four triggered stations with any type of T2 trigger [25]. With the completed array, the global T3 trigger rate is about two events per minute, one third being actual shower events at energies above 3×10^{17} eV.

3. Generalities of UHE Neutrino search

With the SD of the Pierre Auger Observatory we can detect and identify UHE neutrinos in the EeV range and above [26, 27, 28]. The main challenge from the experimental point of view is to identify neutrino-induced showers in the large background of showers initiated by nucleonic cosmic rays. The concept for identification is relatively simple. While protons, heavier nuclei and even photons interact shortly after entering the atmosphere, neutrinos can generate showers initiated deeply into the atmosphere. When considering vertical showers, even the ones initiated by protons or heavy nuclei have a considerable amount of electromagnetic component at the ground ("young" shower front). However, when looking at high zenith angles ($\theta > 75°$) the atmosphere is thick enough (thicker than about three vertical atmospheres) so that the cosmic rays interacting high in the atmosphere have shower fronts dominated by muons at ground ("old" shower front). A neutrino with $\theta > 75°$ interacting deep will present a young shower front and, consequently, can be distinguished.

At the SD level, young showers induce signals spread in time over hundreds of nano-seconds in a fraction of the stations triggered by the shower, while old showers induce narrow signals spreading over typically tens of nano-seconds in practically all the stations of the event. With the 25 ns time resolution of the FADC of the water Cherenkov stations, the distinction between traces induced by young and old shower fronts can be easily accomplished. In Fig. 2 we show an example of those two types of traces.
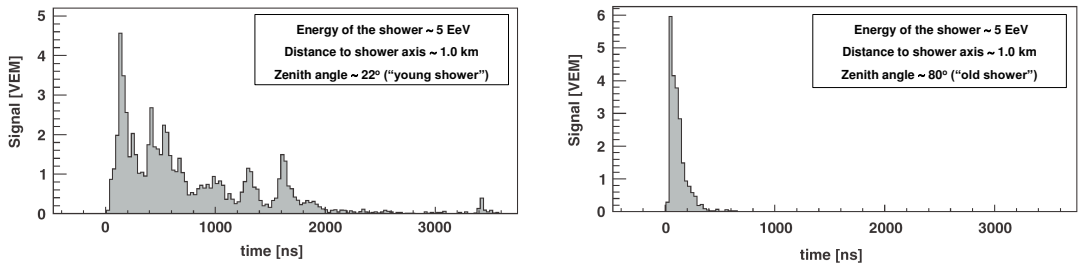
Figure 2: FADC traces of stations at 1 km from the shower core for two real showers of 5 EeV. Left panel: shower arriving in the early stages of development ("young" shower). Right panel: "old" extensive air shower $(\theta \sim 80°)$.

With this simple idea, we can search for two types of neutrino-induced showers at the surface detector array of the Pierre Auger Observatory, namely:

1. Earth-skimming showers induced by tau neutrinos (ν_τ) that travel in the upward direction with respect to the vertical to ground. ν_τ can skim the Earth's crust and interact relatively close to the surface inducing a tau lepton which escapes the Earth and decays in flight in the atmosphere, close to the SD.

   Typically, only Earth-skimming ν_τ-induced showers with zenith angles $90° < \theta < 95°$ may be identified.

2. Showers initiated by any neutrino flavour moving down at large angles with respect to the vertical at ground that interact in the atmosphere close to the surface detector array. We include here showers induced by ν_τ interacting in the mountains surrounding the Pierre Auger Observatory. Although this latter process is exactly equivalent to the "Earth-skimming" mechanism, it is included in this class because such showers are also going downwards. In the following we will refer to all these types of showers as "downward-going" ν-induced showers.

   In this review we restrict ourselves to downward-going ν-induced showers with zenith angles $75° \leq \theta \leq 90°$.

13

In Fig. 3 we show a pictorial representation of the different types of inclined showers that can be detected.
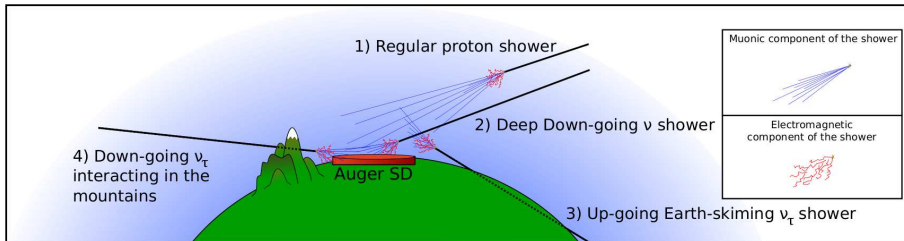

Figure 3: Pictorial representation of the different types of inclined showers that can be detected at the surface detector array of the Pierre Auger Observatory. (1) An inclined shower induced by a proton interacting high in the atmosphere whose electromagnetic component is absorbed and only the muons reach the detector. Inclined showers presenting significant electromagnetic component at the detector level: (2) a deep downward-going ν-induced shower; (3) an Earth-skimming ν_τ interacting in the Earth crust and producing an upward-going τ lepton that decays in flight and induces a shower in the atmosphere; and (4) a ν_τ interacting in the mountains, producing a downward-going τ lepton that decays close to the detector and initiates a shower.

4. Simulation of neutrino showers

Monte Carlo simulations of neutrino-induced showers are crucial to establishing identification criteria and computing the acceptance of the SD to UHEνs. The whole simulation chain is divided in three stages:

1. High energy processes:

   a) The ν-nucleon interaction in the atmosphere for downward-going neutrinos is simulated with HERWIG [29].

   The output of HERWIG includes the types, energies and momenta of the secondary particles produced for both charged (CC) and neutral current (NC) neutrino interactions (see Fig. 4 for a pictorial summary of all the channels considered in this work).

   b) In the case of ν_τ CC interactions, the τ lepton propagation in the Earth and/or in the atmosphere is simulated with a dedicated, fast and flexible code which allows us to easily study the influence on the outgoing τ lepton flux of different ν_τ interaction cross sections, τ energy loss models, etc. The simulation of the decay of

the τ (when necessary) is performed with the TAUOLA package [30].

2. Shower development in the atmosphere:

   The AIRES Monte Carlo code [31] is used to propagate the particles produced in a high energy ν interaction, or in the decay of a τ lepton. The types, energy-momenta and times of the particles reaching the SD level are obtained.

3. Surface detector array simulation:

   This is performed with the $\overline{\text{Off}\underline{\text{line}}}$ software [32]. Firstly particles reaching a surface detector station are injected into the station, and with the aid of GEANT4 [33] the amount of Cherenkov light produced in water is calculated. Then the FADC traces of the PMT signals are obtained, and the total signal due to the particles entering the station, as well as several quantities characterizing the FADC trace which will be relevant for neutrino identification are computed (see below). Also both the local trigger condition (T2 - either Threshold or ToT), and the global trigger condition (T3) are applied to the simulated events in the same way as for collected data.

The phase space of the simulations – namely, neutrino energy, zenith angle of incidence, interaction depth in the atmosphere for downward-going neutrinos, and altitude of the τ decay in the case of Earth-skimming ν_τ – spans a sufficiently wide range of numerical values as to guarantee that at the edges of the phase space none of the simulated showers fulfills the global trigger conditions. This is taken as a clear indication that a complete sample of showers has been produced without introducing any bias and therefore that the Monte Carlo sample correctly represents the characteristic of showers that could trigger the SD of the Pierre Auger Observatory. For the Earth-skimming channel, showers were simulated at zenith angles between 90.1° and 95.9° and at an altitude of the decay point above the Pierre Auger Observatory up to 2500 m. In the case of downward-going neutrinos, simulations were performed at zenith angles in the range 75°–89°.

5. Identifying neutrino-induced showers

As stated above, the selection of potential neutrino-induced showers (neutrino candidates) is based on two steps:

1. Firstly, we select among the data collected at the SD of the Pierre Auger Observatory those events that arrive in inclined directions with respect to the vertical.
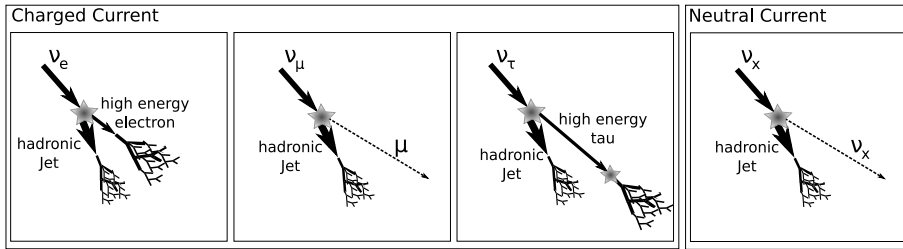
Figure 4: Sketch of the different types of showers induced by UHE neutrinos. All the channels depicted contribute to the neutrino event rate due to downward-going ν induced showers.

2. Secondly, we select among the inclined events those with FADC traces that are spread in time, indicative of the presence of an inclined shower in the early stage of development, a clear signature of a deeply interacting neutrino triggering the SD.

Although the two steps above are the same for all the neutrino-induced showers searched for at the Pierre Auger Observatory, due to the different nature of Earth-skimming and downward-going neutrino induced showers, the criteria and selection cuts that are applied to data are slightly different.

5.1. Selection of inclined events

First of all, events occurring during periods of data acquisition instabilities [25] are excluded.

For the remaining events the FADC traces of the triggered stations are first "cleaned" to remove accidental signals induced (mainly) by atmospheric muons arriving closely before or after the shower front – produced in showers different than the triggering one and which are below the energy threshold of the Pierre Auger Observatory. The trace cleaning procedure is detailed in [27]. After that, the start times of the signals in all stations included in the global trigger are requested to be compatible with a plane shower front moving at roughly the speed of light. This compatibility is realized through upper bounds on both, the largest residual and the mean quadratic residual from the planar fit. If the condition is not fulfilled, fits are attempted removing one station; for this operation, the stations are sorted by increasing *quality* (based on the integrated amplitude and the duration of the signal), and the procedure is stopped as soon as a satisfactory solution is found. If none is found, trials are made removing two stations, and so on. The event is accepted if at least three (four) stations in the Earth-skimming (downward-going) case belong to the configuration.

The second step in both channels is the selection of inclined showers.

16

From the pattern (footprint) of stations at ground (see Fig. 5) we can extract a length L along the arrival direction of the event (i.e., the main axis of the event) and a width W perpendicular to it characterizing the shape of the footprint (see [27] for complete details). The ratio L/W depends on zenith angle. Vertical events have $L/W \sim 1$ and this ratio increases gradually as the zenith angle increases. Very inclined events typically have elongated patterns on the ground along the direction of arrival, and hence large values of L/W. A cut in L/W is therefore a good selector of inclined events. The exact value of this cut is different for downward-going and Earth-skimming events, and was determined through Monte Carlo simulations of ν-induced showers performed at different zenith angles. For downward-going events with $\theta > 75°$ the requirement is $L/W > 3$, while for Earth-skimming it is more restrictive $L/W > 5$ since only quasi-horizontal showers with largely elongated footprints can trigger the array [1] (see Fig. 3 in Ref.[27]).
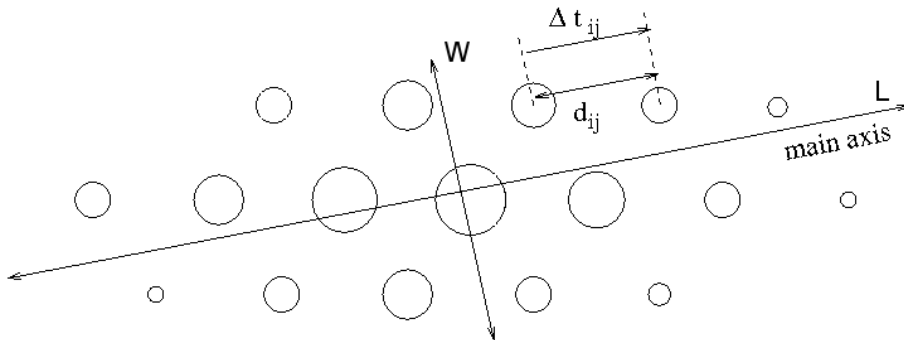
Figure 5: Schematic view of the footprint of a shower triggering the surface detector array of the Pierre Auger Observatory. The shower triggers the array from the left to the right of the figure, along the "main axis". The circles represent the position of the stations, with their sizes being proportional to the collected signal in the PMTs. See text for more details.

Another indication of inclined events is given by the apparent speed V of the trigger from a station i to a station j, averaged over all pairs (i, j) of stations in the event. This observable denoted as $\langle V \rangle$ is obtained in a straightforward manner from the distance between the stations after projection along the "main axis" of the footprint at ground (d_{ij}) as depicted in Fig. 5, and from the difference in trigger times of the stations (Δt_{ij}). Vertical showers have apparent average speeds exceeding the speed of light since all triggers occur at roughly the same time, while in very inclined

---

[1] The axis of Earth-skimming showers travelling in the upward direction does not intersect ground, contrary to the downward-going showers case. For this reason, we exploit the properties of the footprint generated by the shower particles that deviate laterally from the shower axis and trigger the water Cherenkov stations.

events $\langle V \rangle$ is concentrated around the speed of light. Moreover its Root-Mean-Square (RMS(V)) is small. For downward-going (Earth-skimming) events $\langle V \rangle$ is required to be below 0.313 m ns^{-1} ($\langle V \rangle \in [0.29, 0.31]$ m ns^{-1}) and RMS(V)/$\langle V \rangle <$ 0.08 (RMS(V)$<$ 0.08 m ns^{-1}). The values of these selection requirements are based on comparisons between data and Monte Carlo simulations. Also, and only for downward-going events, a further quality cut is applied consisting on a simple reconstruction of the zenith angle θ_{rec} and the requirement that $\theta_{\mathrm{rec}} > 75°$ (see [28] for full details).

In the top part of Table 1 the cuts applied to the observables used to select inclined events are summarized.

	Earth-skimming	Downward-going
	Number of Stations $\geq$ 3	Number of Stations $\geq$ 4
Inclined Showers	- $L/W > 5$ 0.29 m ns^{-1} $<\langle V \rangle<$ 0.31 m ns^{-1} RMS(V) $<$ 0.08 m ns^{-1}	$\theta_{\mathrm{rec}} > 75°$ $L/W > 3$ $\langle V \rangle ~<~$ 0.313 m ns^{-1} RMS(V)/$\langle V \rangle<$ 0.08
Young Showers	At least 60% of stations with ToT trigger & AoP > 1.4	Fisher discriminant $\mathcal{F}$ based on Area-over-Peak (AoP)

Table 1: Observables and numerical values of cuts applied to select *inclined* and *young* showers for Earth-skimming and downward-going neutrinos. See text for explanation.

5.2. Selection of young showers

Once inclined showers are selected the next step is to identify young showers among the data collected at the SD of the Pierre Auger Observatory.

To optimize the numerical values of the cuts and tune the algorithms needed to separate neutrino-induced showers from the much larger background of hadronic showers, we divided the whole data sample into two parts (excluding periods of array instability). A fraction of the data (training period) is dedicated to define the selection algorithm. These data are assumed to be overwhelmingly constituted of background showers. The applied procedure is conservative because the presence of neutrinos would result in a more severe definition of the selection criteria. The remaining fraction is not used until the selection procedure is established, and then it is "unblinded" to search for neutrino candidates. In Table 2 we indicate the periods used for training and "blind" search. The blind search period for the Earth-skimming (downward-going) analysis corresponds to an equivalent of

	Earth-skimming	Downward-going
Training period	1 Nov 04 - 31 Dec 04	1 Jan 04 - 31 Oct 07
Blind search period	1 Jan 04 - 31 May 10	1 Nov 07 - 31 May 10
Equivalent full Auger blind search period	3.5 yr	2.0 yr
ν candidates	0	0
Diffuse limit 90% C.L. (GeV cm^{-2} s^{-1} sr^{-1})	$k < 3.2 \times 10^{-8}$	$k < 1.7 \times 10^{-7}$
Energy range (EeV)	$\sim 0.16 - 20.0$	$\sim 0.1 - 100.0$

Table 2: Training and blind search periods for the search for Earth-skimming and downward-going neutrino candidates. In the 3$^{\rm rd}$ row we indicate the equivalent period of time of a full surface detector array. In the 4$^{\rm th}$ row we give the number of candidates found in the search period after unblindly applying the cuts selecting *inclined* and *young* showers (see Table 1). In the 5$^{\rm th}$ row we give the numerical value of the 90% C.L. limit to the normalization k of a diffuse flux of UHE neutrinos assumed to behave with energy as $dN/dE = k\, E^{-2}$. Systematic uncertainties are included in the value of the limit (see Sec. 6.3 for details). In the last row we indicate the energy range where the limits apply, typically the energy interval where 90% of the events are expected.

~ 3.5 yr (~ 2 yr) of a full surface detector array consisting of 1600 stations working continuously without interruptions.

It is worth remarking that data instead of Monte Carlo simulations of hadronic showers are used to optimize the identification cuts. The first reason for this is that, the composition of the primary UHECR flux – a necessary input in the simulations – is not accurately known. Also, the detector simulation may not account for all possible detector defects and/or fluctuations that may induce events that constitute a background to UHE neutrinos, while they are accounted for in collected data, including those which are not well known, or even not yet diagnosed.

This is the general strategy followed in the search for Earth-skimming ν_τ and downward-going ν-induced showers. However the two searches differ in several aspects that we detail in the following sections.

5.2.1. Earth-skimming analysis

In the Earth-skimming analysis we identify young showers by placing a cut on the fraction of stations in the event that fulfill two conditions: (1) the station passes the ToT local trigger condition, and (2) the ratio of

the integrated signal over the peak height – the so-called Area-over-Peak (AoP), a variable that carries information on the time spread of the signal – is greater than 1.4. By convention, both the "area" and the "peak" values are normalized to 1 in signals induced by isolated muons.

The aim of both conditions is to identify broad signals in time such as those induced by showers developing close to the array. In particular, with the second condition we reject background signals induced by inclined hadronic showers, in which the muons and their electromagnetic products are concentrated within a short time interval, exhibiting AoP values close to the one measured in signals of isolated muons.

In order to reject inclined hadronic events, at least 60% of the triggered stations in the event are required to fulfill the two conditions above (Table 1). The selection conditions were optimized using data collected during the training period indicated in Table 2. It is important to remark that this is the same selection procedure and training period as in previous publications [26, 27], which is applied in this work to a larger data set. The final choice of the actual values of the neutrino selection cuts was done by requiring zero background events in the training data sample. When the Earth-skimming cuts in Table 1 are applied blindly to the data collected during the search period, no events survived.

5.2.2. Downward-going analysis

In the search for downward-going events, the discrimination power is optimized with the aid of a multi-variate technique known as the Fisher discriminant method [34]. The method consists on constructing a linear combination of observables denoted as $\mathcal{F}$ which optimizes the separation between two samples of events, in our case background hadronic inclined showers occuring during the downward-going training period (see Table 2), and Monte Carlo simulated ν-induced showers. The method requires as input a set of variables which can discriminate between the two samples. For that purpose we use variables depending on the Area-over-Peak (AoP) – as defined above – of the FADC traces. In the first few stations hit by a deep inclined shower, the typical AoP values range between 3 and 5 (left-hand panel of Fig. 6).

After training the Fisher method, a good discrimination is found when the following ten variables are used to construct the linear Fisher discriminant variable $\mathcal{F}$: the AoP of the four stations that trigger first (early stations) in each event, their squares, the product of the four AoPs, and a global parameter that measures the asymmetry between the average AoP of the early stations and those triggering last (late stations) of the event.

The product of the AoP of the earliest four stations in the event aims at minimizing the relative weight of an accidentally large AoP produced, for instance, by a single muon which does not belong to the shower front
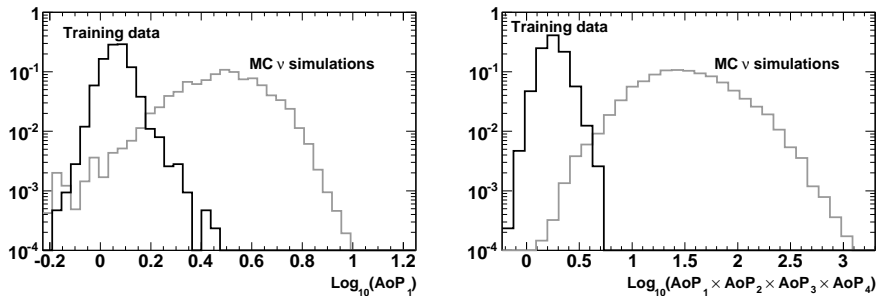
20

Figure 6: Distributions of the Area-over-Peak (AoP, see text) of the earliest station (left) and of the product of the AoP of the first four stations in the event (right). In each panel we show the distribution of the corresponding variable in background events (i.e. data events in the training sample as indicated in Table 2), and in simulated electron neutrino charged-current events. These are two of the ten variables depending on the AoP used in constructing the multi-variate Fisher discriminant linear polynomial to optimize the separation between background and neutrino-induced showers. See text for more details on the remaining 8 variables.

arriving at a station before or after the shower itself. This variable is also a very good discriminator as shown in the right-hand panel of Fig. 6. We have also checked in Monte Carlo simulations that neutrino-induced events typically have an asymmetry parameter larger than proton or nucleus-induced showers.

As the shower front is broader at larger distance from the core for both young and old showers, the discrimination is better when splitting the samples according to the number of selected stations N. A Fisher discriminant polynomial was obtained separately for $4 \leq N \leq 6$, $7 \leq N \leq 11$, and $N \geq 12$. An excellent separation is achieved for events in each of the three sub-samples. The individual AoPs of the first four tanks have the largest weights in the Fisher polynomials. In Fig. 7 we show as an example the distribution of $\mathcal{F}$ in the sub-sample with the smallest number of selected stations (the distributions corresponding to the three sub-samples can be found in Fig. 7 of [28]).

Once the Fisher discriminant $\mathcal{F}$ is defined, the next step is to define a numerical value of $\mathcal{F}$, denoted as $\mathcal{F}_{\text{cut}}$, that separates neutrino candidates from regular hadronic showers. One of the advantages of the Fisher discriminant method is that it allows us to estimate the expected rate of background events, and hence to tune the value of $\mathcal{F}_{\text{cut}}$ so that the background is kept at a very low value. This is important given the fact that the expected rate of detected neutrino events will be small. Data in the training period
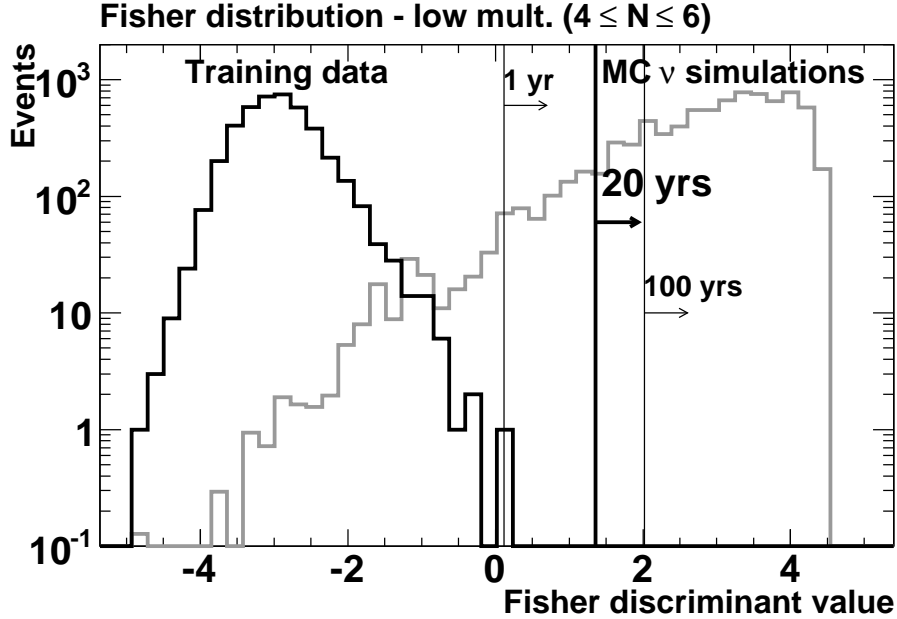
Figure 7: Distribution of the value of the Fisher polynomial ($\mathcal{F}$, see text for details) for events with number of selected stations $4 \leq N \leq 6$. Data in the training period (see Table 2) describe the nucleonic background, while Monte Carlo simulated downward-going neutrinos correspond to the signal. The vertical lines indicate $\mathcal{F}_{\mathrm{cut}}$ needed to expect 1 event in the labeled periods of time (full SD array).

indicated in Table 2 was exploited to produce a reasonable prediction of the background (see [28] for full details). In practice, we fix $\mathcal{F}_{\mathrm{cut}}$ so that the estimated number of background events is 1 in 20 yr of data taking by a full Auger SD. With this cut, and for our search sample we have an estimated background of 0.1 events for each multiplicity class that add up to a total of 0.3 events with a statistical uncertainty of 30%. It is important to re-mark that this estimate relies on the a priori hypothesis that the background has an exponential distribution in $\mathcal{F}$. Given the fact that we do not have a solid estimation of the actual background, a conservative approach was taken assuming the background is zero, in other words, the estimated 0.3 background events were not used to improve our upper limit on the flux [37] (see Sec. 7.1 below).

As exemplified in Fig. 7 for the low multiplicity events, the identifica-tion cuts reject only $\sim 10\%$ of the simulated neutrino events, and those are mainly neutrinos interacting far from the ground that, being similar to

nucleonic-induced showers, are not expected to be identified.

Finally, when the downward-going cuts in Table 1 are applied to the data collected during the search period, no neutrino candidates appeared (see Table 2).

6. Exposure to UHE neutrinos

6.1. Neutrino identification efficiencies

With the criteria to select neutrino-induced showers indicated in Table 1, we obtain a relatively large identification efficiency both for Earth-skimming ν_τ and downward-going ν-induced showers. The efficiency has been computed with Monte Carlo simulations as the fraction of simulated events identified as neutrinos.

In the case of Earth-skimming ν_τ induced showers, and a full Auger SD working without interruption, the efficiencies depend only on the energy of the emerging τ leptons (E_τ) and on the altitude of the "center of the shower" (h_c) above ground (averaged over the decay channels). This is conveniently defined as the altitude of the shower axis at a distance of 10 km away from the τ decay point along the shower axis. Showers induced by τ leptons with the same energy but with different zenith angles – the range in θ being very narrow – have approximately the same efficiency as long as the corresponding altitudes of their shower maxima h_c are the same. The maximum efficiency that can be reached is 82.6%, the 17.4% remaining corresponds to the channel in which the τ decays into a μ which is unlikely to produce a detectable shower close to ground. In Fig. 8 we show the trigger and identification efficiencies as a function of h_c for different τ energies. As expected, the efficiency increases with E_τ and drops as the τ decays at increasing altitude from ground.

In the case of downward-going neutrinos the identification efficiency depends on neutrino flavour, type of interaction (CC or NC), neutrino energy (E_ν), zenith angle (θ), and distance (D) measured from ground along the shower axis at which the neutrino is forced to interact in the simulations. An example of the efficiency that can be achieved in a full SD array is shown in Fig. 9. The efficiency is different from zero between a minimal depth close to ground (a minimal amount of matter needed for the ν-induced shower to reach a sufficient lateral expansion), and a maximal one (such that the electromagnetic component is almost extinguished at ground level and hence the neutrino cannot be identified). The efficiency as well as the slice of atmosphere where it is different from zero, typically increase with neutrino energy, and depend on the neutrino flavour and interaction. As an extreme example, high energy ν_τ interacting in the atmosphere through the CC channel can be identified regardless of the interaction depth in the atmosphere, as long as the energetic τ produced in the interaction decays and produces

a shower close to ground.

6.2. Exposure

Ideally, for the calculation of the exposure of the SD of the Auger Observatory to ultrahigh energy neutrinos, the simulated neutrino showers should be randomly distributed over the actual configurations of the array, applying to the shower at ground the trigger and neutrino identification conditions to obtain the active (effective) area of the array at every second, and as a function of the parameters of the neutrino-induced showers (neutrino energy, zenith angle, h_c,...). A sum over time and integration in solid angle would then yield the *exposure* ($\mathcal{E}$) to UHE neutrinos in both the Earth-skimming and downward-going neutrino analyses. During the search periods considered for both Earth-skimming and downward- going neutrino searches, the surface detector array of the Pierre Auger Observatory was growing continuously. Since the number of working stations and their status are monitored every second, we know with very good accuracy the SD configuration at any instant as well as its evolution with time.

In practice, to avoid having to cope with an unaffordable number of configurations, different strategies were devised to calculate in an accurate and less time-consuming manner the effective area of the SD array to Earth-skimming and downward-going ν-induced showers.

For downward-going neutrinos, the calculation of the exposure involves folding the SD array aperture with the ν interaction probability and the identification efficiency, and integrating in time. Changes in the configuration of the array introduce a dependence of the efficiency ϵ on the position of the core of the shower $\vec{r} = (x, y)$ in the surface S covered by the array, and on time t.

Assuming a 1:1:1 flavour ratio (as expected due to the effects of neutrino oscillations during propagation from the sources), the total exposure can be written as [28]:

$$\mathcal{E}^{\mathrm{DG}}(E_\nu) = \frac{2\pi}{m} \sum_i \left[\sigma^i(E_\nu) \int \, dt \, d\theta \, dD \right.$$
$$\left. \sin\theta \, \cos\theta \, A_{\mathrm{eff}}^i(\theta, D, E_\nu, t) \right] \tag{1}$$

where the sum runs over the three neutrino flavours and the CC and NC interactions, with σ^i the corresponding ν-nucleon interaction cross-section [35] and m the nucleon mass. The integral is performed over the zenith angle θ, the interaction depth D of the neutrino (in units of g cm^{-2}), and the blind search period. A_{eff}^i is the effective area of the SD array given by:

$$A_{\mathrm{eff}}^i(E_\nu, \theta, D, t) = \int \epsilon^i(\vec{r}, \theta, D, E_\nu, t) \, dA \tag{2}$$

24

where the integral is performed over the core positions $\vec{r}$ of the showers.

For the Earth-skimming neutrinos the calculation of the exposure is described in [27].

The exposures obtained for the search periods indicated in Table 2 are plotted in Fig. 10, where for the downward-going neutrino induced showers we also plot the contribution of the different channels (Fig. 4) to the total exposure. Among them we have included the possibility that downward-going ν_τ interact with the mountains surrounding the Observatory which provide a dense target for neutrino interactions.

The exposure to Earth-skimming neutrinos is higher than that to downward-going neutrinos by a factor between ~ 2 and ~ 7 depending on the neutrino energy, partially due to the longer search period in the Earth-skimming analysis ~ 3.5 yr of full Auger, compared to ~ 2.0 yr in the case of the downward-going analysis. When normalized to the same search time, the Earth-skimming channel is still a factor $\sim 2.5 - 3$ more sensitive when integrated over the whole energy range, mainly due to the larger density of the Earth's crust where ν_τ interactions can occur, compared to the atmosphere. The larger number of neutrino flavours and interaction channels that can be identified in the downward-going analysis, as well as the broader angular range ($75° < \theta < 90°$ compared to $90° < \theta < 95°$), partly compensate the difference.

6.3. Systematic Uncertainties

Several sources of systematic uncertainty have been carefully considered. Some of them are directly related to the Monte Carlo simulation of the showers, i.e., generator of the neutrino interaction either in the Earth or in the atmosphere, parton distribution function, air shower development, and hadronic model. Others have to do with the limitations on the theoretical models estimating, for instance, the interaction cross-section or the τ energy loss at high energies. Some of these sources play a dominant role on the Earth-skimming analysis, while others do on the downward-going neutrino one.

In both analyses the procedure to incorporate the systematic uncertainties is the same. Different combinations of the various sources of systematic uncertainty render different values of the exposure, and the final uncertainty is incorporated in the value of the limit itself through a semi-Bayesian extension [36] of the Feldman-Cousins approach [37]. In Table 3 we summarize the dominant sources of systematic uncertainty and their impact on the exposure. In the Earth-skimming analysis the model of energy loss for the τ is the dominant source of uncertainty, since it determines the energy of the emerging τs after propagation in the Earth; the impact of this on the downward-going analysis is much smaller since τ energy losses are only relevant for ν_τ interacting in the mountains, a channel that is estimated to

Source of uncertainty	Earth-skimming	Downward-going
Monte Carlo simulation of shower	$+20\%, -5\%$	$+9\%, -33\%$
ν-nucleon cross-section	$+5\%, -9\%$	$+7\%, -7\%$
τ energy losses	$+25\%, -10\%$	$+6\%, -6\%$
Topography	$+18\%, 0\%$	$-$

Table 3: Main sources of systematic uncertainty and their impact on the Earth-skimming [27] and downward-going [28] exposures.

contribute only $\sim 15\%$ to the total exposure. The uncertainty on the shower simulation, that stems mainly from the different shower propagation codes and hadronic interaction models that can be used to model the high energy collisions in the shower, contributes significantly in both cases. The presence of mountains around the Observatory – which would increase the target for neutrino interactions in both cases – is explicitly simulated and accounted for when obtaining the exposure of the SD to downward-going neutrino-induced showers, and as a consequence does not contribute directly to the systematic uncertainties. However, it is not accounted for in the Earth-skimming limit shown in Table 2. Instead, we take the topography around the Observatory as a source of systematic uncertainty and we estimated that accounting for it would have increased the event rate by $\sim 18\%$ (Table 3).

7. Results

We have searched for neutrino candidates over the search data periods and no events fulfilling either the Earth-skimming or the downward-going selection cuts were found. This allows us to put limits to the UHE diffuse neutrino flux.

7.1. Limits to the diffuse flux of UHE neutrinos

Under the assumption that the UHE neutrino flux $\Phi(E)$ behaves with neutrino energy as:

$$\Phi(E) = \frac{dN}{dE} = k \; E^{-2} \qquad [\text{GeV}^{-1} \; \text{cm}^{-2} \; \text{s}^{-1} \; \text{sr}^{-1}] \; , \qquad (3)$$

the *integrated* limit on the value of k is:

$$k = \frac{N_{\text{up}}}{\int_{E_{\text{min}}}^{E_{\text{max}}} \; E^{-2} \; \mathcal{E}(E) \; dE} \qquad (4)$$

where $\mathcal{E}(E)$ is the exposure. The actual value of the upper limit on the signal events (N_{up}) depends on the number of observed and expected background

events. We recall here that, according to [37], $N_{\mathrm{up}} = 2.44$ at 90% C.L. for zero candidates and no expected background events. When systematic uncertainties are included (Sec. 6.3) the value of N_{up} changes.

The final limits are reported in Table 2 where we give the normalization k obtained in the search periods (indicated in the same table) for the Earth-skimming and downward-going searches.

In Fig. 11 we show the Earth-skimming and downward-going integrated neutrino flux which indicate the level of a diffuse neutrino flux assumed to behave with energy as E^{-2}, needed to detect N_{up} events with a Poisson probability of $\sim 90\%$ given the exposure accumulated during the 3.5 years for Earth-skimming neutrinos (2.0 years for downward-going) of equivalent time of a full SD.

Another way of presenting the results is to display the upper limit in differential form. In this procedure we assume that the diffuse neutrino flux behaves as E^{-2} within energy bins of 0.5 width on a decimal logarithmic scale, and is given by $2.44/(0.5 \log(10) \cdot E \cdot \mathcal{E}(E))$, assuming again no background. The differential limit obtained in this way is shown in Fig. 11 for the Earth-skimming and downward-going cases. We achieve most ($\sim 90\%$) of the sensitivity in the energy range $\sim 0.16 - 20$ EeV ($\sim 0.1 - 100$ EeV) for Earth-skimming (downward-going) neutrinos. In Fig. 11 we also show several predictions of different theoretical models of cosmogenic neutrino production [40, 10]. Predictions for cosmogenic neutrino fluxes depend on several unknown parameters including the evolution with redshift of the sources and the injected UHECR composition. Given the uncertainties in these parameters, and in particular the possible presence of heavy primaries in the UHECR spectrum [41], we have plotted a range of models to illustrate the wide range of predictions available [10].

7.2. Event rate predictions

In Table 4 we give the expected number of events from a diffuse flux of cosmogenic neutrinos (produced in the interaction of cosmic ray protons with background radiation fields) [40], from a model of neutrino production through the bottom-up mechanism in Active Galactic Nuclei (AGN) [42], and from a theoretical model [43] in which neutrinos are the product of the decay of super-heavy relic particles of the early stages of the Universe. Optimistic theoretical flux predictions for cosmogenic neutrinos are within reach of our present sensitivity and some models of neutrinos produced in accelerating sources are already being constrained. Exotic models are severely disfavored. Note that all such top down models are also tightly constrained by the limits of the Pierre Auger Observatory on the photon fraction in UHECR [44].

Model & reference	Earth-skimming	Downward-going
Cosmogenic (Fermi) [40]	~ 0.6	~ 0.1
AGN [42]	~ 5.1	~ 0.8
Exotic (SH relics) [43]	~ 3.0	~ 1.0

Table 4: Number of expected events for several theoretical models of UHE neutrino production, given the exposure of the surface detector array of the Pierre Auger Observatory to Earth-skimming and downward-going neutrinos (Table 2).

8. Summary and Prospects

In this paper we have reviewed the searches for astrophysical sources of ultrahigh energy neutrinos at the Pierre Auger Observatory [26, 27, 28].

The neutrino detection technique is based on the observation of extensive air showers induced by downward-going neutrinos of all flavours as they interact with the atmosphere, and by upward-going ν_τ's through the Earth-skimming mechanism. These ν-induced showers display characteristic features that allow us their identification in the overwhelming background of regular UHE hadronic showers. At ground level, high zenith angle neutrino events would have a significant electromagnetic component leading to a broad time structure of detected signals in the surface detector array, in contrast to nucleonic-induced showers.

We have shown that, using Monte Carlo simulations and training data samples, identification criteria for UHE neutrinos can be defined and used to perform a blind search on the remaining data sample. The analysis of the collected data at the Pierre Auger Observatory until 31 May 2010 reveals no candidate events for either downward-going or Earth-skimming neutrinos. Based on this negative result, stringent limits have been placed on the diffuse flux of UHE neutrinos. Even though the Auger Observatory was designed to measure properties of UHECRs, the limits reported in Table 2 provide at present one of the most sensitive bounds on neutrinos at EeV energies, which is the most relevant energy to explore the predicted fluxes of cosmogenic neutrinos.

There are several lines of work in progress inside the Auger Collaboration related to the neutrino search which will be the subject of future reports. Some of the efforts concentrate on the combination of the downward-going and Earth-skimming channels into a single analysis. This will simplify the search procedure and will obviously translate into an improvement of the diffuse neutrino limit. The extension of the downward-going neutrino search to lower zenith angles ($\theta < 75°$) is also very promising. Exploring the sky down to $\theta \sim 60°$ implies a sizeable increase on the exposure and hence on

the limit in case no candidates are found. The main drawback of decreasing θ is that the atmosphere slant depth reduces and nucleonic-induced showers look "younger" when arriving at ground, making their separation from ν-induced showers more challenging. On the other hand, the sensitivity to neutrino detection could also be extended to lower energies by reducing the separation between SD stations. Monte Carlo studies indicate that using a configuration of stations similar to the currently existing "infill" array (~ 60 stations spaced by 750 m) would lead to a significant increase of the neutrino detection probability at lower energies (below 0.3 EeV) with respect to the standard SD array. Nevertheless, due to the small size of the current infill array, the exposure does not appear to be competitive.

Finally, it is worth mentioning that the sensitivity of the Pierre Auger Observatory to the detection of UHEνs from potential astrophysical *point-like* sources is being evaluated. The absence of candidates in the searches for diffuse neutrino fluxes described in this report allows us to place limits on the neutrino fluxes coming from sources in the field of view of the SD of the Auger Observatory. Preliminary results indicate that with the SD we are sensitive to a large fraction of the sky spanning $\sim 100°$ in declination [45].

9. Acknowledgements

References

[1] M. Nagano and A. A. Watson, Rev. Mod. Phys. **72**, 689 (2000).

[2] K. Kotera and A. Olinto, Annu. Rev. Astron. Astrophys. **49**, 119 (2010).

[3] F. Halzen and D. Hooper, Rep. Prog. Phys. **65**, 1025 (2002).

[4] J. K. Becker, Phys. Rep. **458**, 173 (2008).

[5] P. Bhattacharjee and G. Sigl, Phys. Rep. **327**, 109 (2000).

[6] K. Greisen, Phys. Rev. Lett. **16**, 748 (1966);
G. T. Zatsepin and V. A. Kuzmin, Pis'ma ZhZhurnal Eksperimental noi i Teoreticheskoi Fiziki **4**, 114 (1966), JETP Lett. **4**, 78 (1966) (Engl. Transl.).

[7] V. S. Berezinsky and G. T. Zatsepin, Phys. Lett. B **28**, 423 (1969).

[8] R. U. Abbasi *et al.* [HiRes Collaboration], Phys. Rev. Lett. **100**, 101101 (2008).

[9] J. Abraham *et al.* [Pierre Auger Collaboration], Phys. Rev. Lett. **101**, 061101 (2008); J. Abraham *et al.* [Pierre Auger Collaboration], Phys. Lett. B **685**, 239 (2010).

[10] K. Kotera, D. Allard and A. Olinto, JCAP **10**, 013 (2010).

[11] D. Seckel and T. Stanev, Phys. Rev. Lett. **95**, 141101 (2005).

[12] D. Allard *et al.*, JCAP **09**, 005 (2006).

[13] B. Baret and V. Van Elewyck, Rep. Prog. Phys. **74**, 046902 (2011).

[14] L. A. Anchordoqui and T. Montaruli, Annu. Rev. Nucl. Part. Sci. **60**, 129 (2010).

[15] E. Zas, New J. Phys. **7**, 130 (2005).

[16] V. S. Berezinsky and A. Yu. Smirnov, Astrophys. Space Sci. **32**, 461 (1975).

[17] T. Hara *et al.*, Proceedings 11th Int. Cosmic Ray Conf. (Budapest) Acta Phys. Acad. Sci. Hung. **29** (Suppl 3), 361 (1970); M. Nagano *et al.*, J. Phys. Soc. Japan **30**, 33 (1971).

[18] A. M. Hillas *et al.*, Proceedings 11th Int. Cosmic Ray Conf. (Budapest) Acta Phys. Acad. Sci. Hung. **29** (Suppl 3), 533 (1970); D. Andrews *et al.*, Acta Phys. Acad. Sci. Hung. **29**, 337 (1970).

[19] J. Abraham *et al.* [Pierre Auger Collaboration], Nucl. Instrum. Meth. A **523**, 50 (2004).

[20] K. S. Capelle *et al.*, Astropart. Phys. **8**, 321 (1998); P. Billoir *et al.*, Proceedings of NOW 2006, Lecce, Italy.

[21] X. Bertou *et al.*, Astropart. Phys. **17**, 183 (2002).

[22] D. Fargion, Astrophys. J. **570**, 909 (2002).

[23] I. Allekotte *et al.*, Nucl. Instrum. Meth. A **586**, 409 (2008).

[24] X. Bertou *et al.*, Nucl. Instrum. Meth. A **568**, 839 (2006).

[25] J. Abraham *et al.* [Pierre Auger Collaboration], Nucl. Instrum. Meth. A **613**, 29 (2010).

[26] J. Abraham *et al.* [Pierre Auger Collaboration], Phys. Rev. Lett. **100**, 211101 (2008).

[27] J. Abraham *et al.* [Pierre Auger Collaboration], Phys. Rev. D **79**, 102001 (2009).

[28] P. Abreu *et al.* [Pierre Auger Collaboration], Phys. Rev. D **84**, 122005 (2011).

[29] G. Corcella *et al.*, HERWIG 6.5, JHEP **01**, 010 (2001).

[30] S. Jadach *et al.*, Comput. Phys. Commun. **76**, 361 (1993).

[31] S. J. Sciutto, *arXiv:astro-ph/9911331* (software and documentation downloadable from *http://www2.fisica.unlp.edu.ar/auger/aires/ppal.html*)

[32] S. Argirò *et al.* [Pierre Auger Collaboration – The $\overline{\text{Off}}\underline{\text{line}}$ group], Nucl. Instrum. Meth. A, **580**, 1485 (2007).

[33] *http://geant4.web.cern.ch/geant4/*

[34] R. Fisher, Ann. Eugenics **7**, 179 (1936).

[35] A. Cooper-Sarkar and S. Sarkar, JHEP **01**, 075 (2008).

[36] J. Conrad *et al.*, Phys. Rev. D **67**, 12002 (2003).

[37] G. J. Feldman and R. D. Cousins, Phys. Rev. D **57**, 3873 (1998).

[38] R. Abbasi *et al.* [IceCube Collaboration], Phys. Rev. D **83**, 092003 (2011).

[39] P. W. Gorham *et al.* [ANITA Collaboration], Phys. Rev. Lett. **103**, 051103 (2009);
P. W. Gorham *et al.* [ANITA Collaboration], Astropart. Phys. **32**, 10 (2009).

[40] M. Ahlers *et al.*, Astropart. Phys. **34**, 106 (2010).

[41] P. Abreu *et al.* [Pierre Auger Collaboration], Phys. Rev. Lett. **104**, 091101 (2010).

[42] J. K. Becker *et al.*, Astropart. Phys. **23**, 355 (2005).

[43] O. Kalashev *et al.*, Phys. Rev. D **66**, 063004 (2002).

[44] J. Abraham *et al.* [Pierre Auger Collaboration], Astropart. Phys. **31**, 399 (2009).

[45] P. Abreu *et al.* [Pierre Auger Collaboration], Astrophysical Journal Letters, vol. 755 (2012) L4.
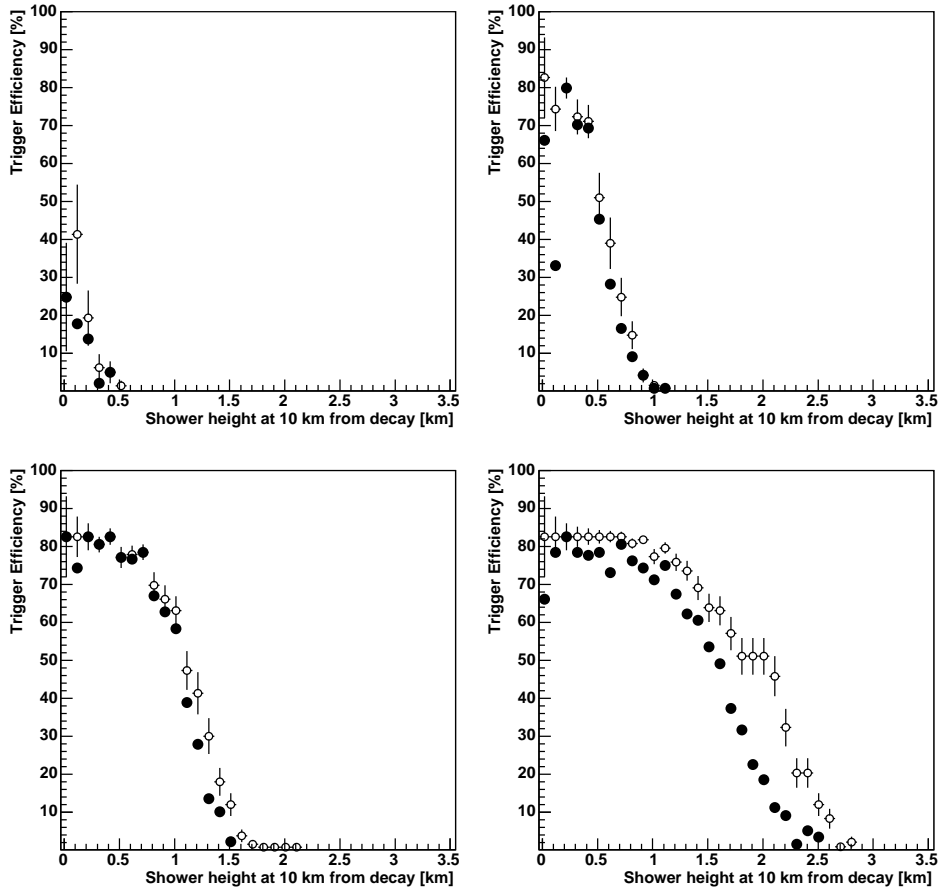
Figure 8: T3 trigger (open dots) and identification (closed dots, cuts as in Table 1) efficiency in the Earth-skimming analysis, as a function of the height above ground of the shower at 10 km from the τ decay point h_c. The efficiency is shown for Monte Carlo showers induced by τs with energy (clockwise from the top left panel) 0.1, 1, 10 and 100 EeV. The efficiencies are calculated in a full SD array (see text for details).
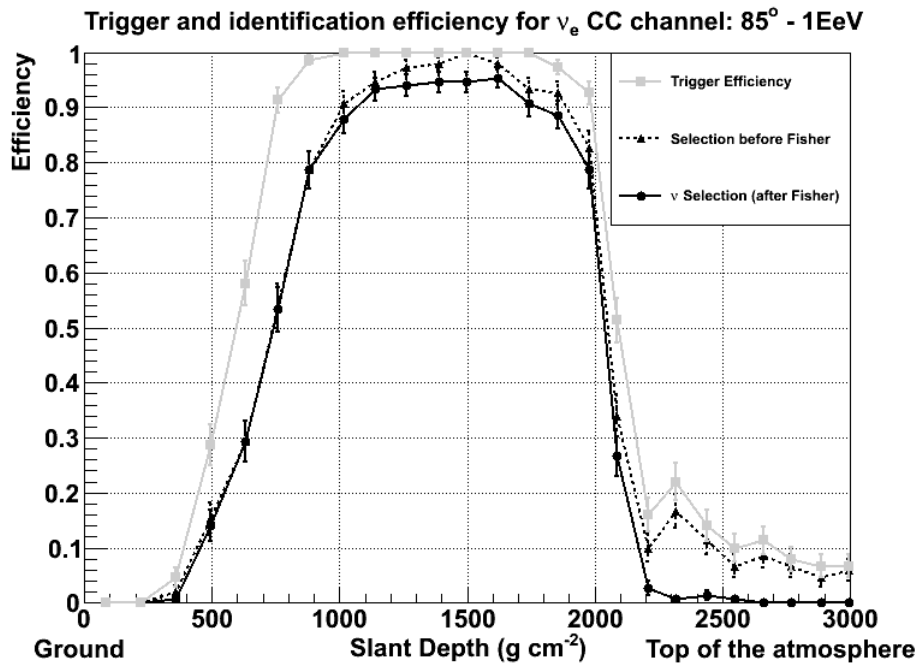
33

Figure 9: Fraction of electron neutrinos of energy 1 EeV and $\theta = 85°$ triggering the array (solid grey line) and passing the downward-going analysis cuts in the second column of Table 1 (solid black line) as a function of the slant depth of the interaction above the ground. The dashed line represents the fraction of events passing all cuts except for the cut on the Fisher discriminant $\mathcal{F}$ (see Sec. 5.2). The efficiencies are calculated in a full SD array (see text for details).
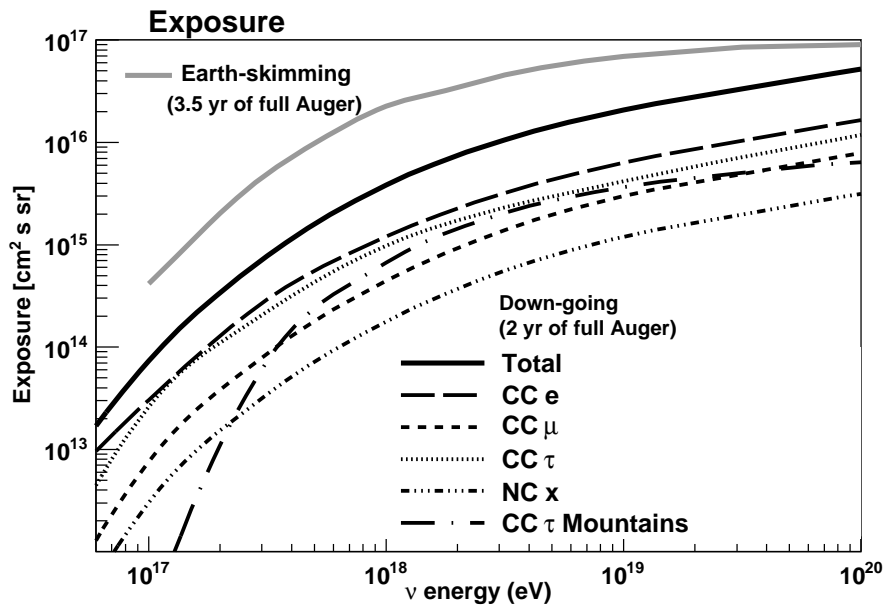
Figure 10: Exposure of the surface detector array of the Pierre Auger Observatory on the data search periods to Earth-skimming ν-induced showers (equivalent to 3.5 yr of full Auger), and to downward-going ν-induced showers (equivalent to 2 yr of full Auger).
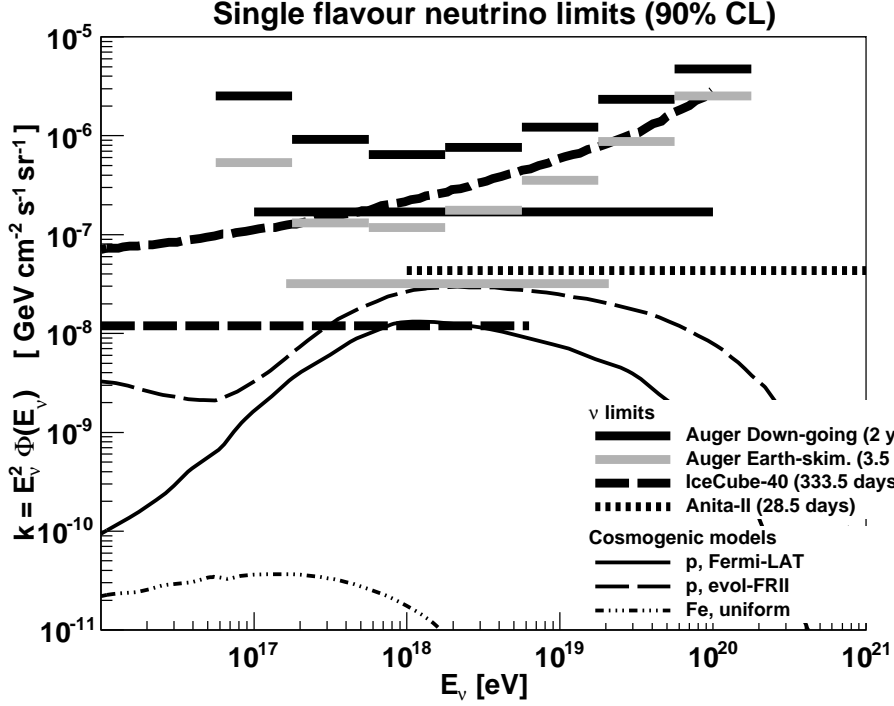
Figure 11: Thick lines: Differential and integrated upper limits (at 90% C.L.) to the diffuse flux of UHE neutrinos (single flavour assuming equipartition) from the Pierre Auger Observatory for downward-going ν (equivalent search period = 2 yr of full Auger) and Earth-skimming ν_τ (equivalent search period = 3.5 yr of full Auger). Limits from other experiments are also plotted [38, 39]. All limits have been scaled to single flavour. The IceCube differential limit is scaled by a factor 1/2 due to the different binning in energy with respect to the Auger differential limits.

Thin lines: Expected fluxes for three theoretical models of cosmogenic neutrinos (scaled to single flavour when necessary). "p, Fermi-LAT" [40] corresponds to the best fit to UHECR spectrum incorporating Fermi-LAT bound assuming that the transition from Galactic to extragalactic CRs takes place at 10^{19} eV. "p, evol-FRII" [10] assumes the FRII strong source evolution with a pure proton composition, dip transition model and maximum energy of UHECRs at the sources $E_{p,\mathrm{max}} = 10^{21.5}$ eV. "Fe, uniform" [10] represents an extreme model assuming an iron rich composition, low $E_{p,\mathrm{max}}$, uniform evolution of the UHECR sources case.